Arch. Mech., **55**, 5–6, pp. 407–430, Warszawa 2003

The process zone around the tip of cracks in metal matrix composites

S. K. KOURKOULIS

National Technical University of Athens,
School of Applied Sciences, Department of Mechanics,
Theocaris Building, Zografou Campus, GR 157-73 Athens, Hellas
e-mail:stakkour@central.ntua.gr

SOME CHARACTERISTICS of the process zone developed around the tips of cracks as well as the fractography of the fracture surfaces constitute the subject of the present paper. The study was carried out using Scanning Electron Microscopy for the determination of the Crack Tip Opening Displacement, while numerical analysis and experimental results were combined for the determination of the J-integral. A modern particulate Metal Matrix Composite and its matrix alloy were used for the fabrication of relatively thin tensile specimens of two different types, i.e. single- and double-edge-notched. Dependence of the above quantities on the thickness of the specimen is detected: both the critical Crack Tip Opening Displacement and the critical J-integral are found to increase in an almost linear manner with thickness. For comparison, intact prismatic specimens were considered, in order to study the dependence of ductility and fracture on the thickness of the specimen. It is observed that they depend also on the specimen thickness in a similar manner. Variation of these two properties with the direction of the specimen with respect to the rolling axis is also detected, indicating the importance of the plastically induced anisotropy due to the manufacturing process. Concerning the mechanisms leading to failure, it is concluded that void coalescence is active although void nucleation due to the presence of particles appears to be unavoidable.

1. Introduction

THE QUANTIFICATION of the characteristics of the process zone developed around the tip of a crack is among the most important tasks of Fracture Mechanics since this zone governs the further development and propagation of the crack. However, in spite of the fact that the definition of a single-parameter mechanical quantity, which could serve as a failure criterion in case of pre-cracked specimens or structural members, has been the subject of an enormous number of research papers, already since the very early steps of the development of Fracture Mechanics, the problem is not yet closed.

The introduction of the concept of the stress intensity factor, K, by WESTERGAARD [1] and IRWIN [2] as well as of the concept of the critical stress intensity factor or fracture toughness, K_C, gave the impression that an acceptable solution

of the problem was achieved. The initial enthusiasm was shadowed, however, by a long series of experimental findings, which indicated that K_C depends on the thickness of the specimen [3]. Indeed, experiments have shown that only above a certain specimen thickness, beyond which the material is under predominantly plane strain, K_C tends to a constant value, which is usually considered as a material property. Below this limit K_C depends in a sigmoid manner on the thickness of the specimen exhibiting a well-defined maximum value. For very thin specimens the dependence is not exactly known.

The above behaviour is usually attributed to the fact that for very thin plates, the fracture toughness results from the plastic energy spent in the neck in front of the crack tip, which in general is significantly larger in comparison to the energy spent for the overall damage of the material. The work of necking, however, depends directly on the thickness of the specimen. As a consequence, the fracture toughness varies also with thickness, as pointed out by BLUHM [4] and SWEDLOW [5] already from the early sixties and for purely plane stress the variation is almost linear.

Unfortunately, experimental results concerning the dependence of fracture toughness on thickness for very thin specimens are rather scarce and as a result, the relation between the resistance to cracking initiation and plate thickness remains insufficiently understood until today [6] even for conventional metallic materials and alloys. The situation is worse in case of modern composite materials and especially for the class of them described under the term particulate Metal Matrix Composites (MMCs), since the study of their behaviour from the Fracture Mechanics point of view is still in progress all over the world. These materials were only developed during the last two or three decades to meet the increased demands of aerospace industry for optimized mechanical properties combined with low specific weight.

In general, the principal concept of the technology of composite materials is to combine certain assets of their constituents in order to give to the newly synthesized material unique and useful properties. The reinforcement may be either of one- (fibrous) or two- (laminar) or even three-dimensional shape (particulates). The last class includes composites with more than 20% of the hard reinforcing dispersed phase. The particulate composites are non-homogeneous materials and their properties appear to be very sensitive to the constituent properties as well as to the geometric shapes of the array. The strength of particulate composites depends on the diameter of the particles, the interparticle spacing as well as on the volume fraction of the reinforcement.

Among particulate composite materials Metal Matrix Composites (MMCs) are advantageous as structural materials since in their virgin state they are isotropic materials without any kind of texture anisotropy. Also, they combine metallic with ceramic properties, such as high strength, high modulus of elastic-

ity, high toughness, relatively low sensitivity to thermal shocks and temperature changes, high surface durability, low sensitivity to surface flaws, high thermal and electrical conductivity. Additionally, the ductile metal matrices, such as aluminum (used in the present work), titanium or nickel-chromium alloys, undergo energy absorbing plastic deformation under impact, which is very important in many dynamic structural applications [7].

On the other hand, the ductile matrix permits the blunting of cracks and relieves stress concentrations by plastic deformation. It is thus expected that the composite materials should be characterized by improved fracture toughness. However, it has been pointed out [8] that the presence of cracks strongly deteriorates the fracture strength of MMCs, in comparison to the uncracked materials, rendering the use of the matrix material more advantageous in case of presence of macro-cracks. Indeed, pairs of matrix alloys and MMCs are reported for which under specific loading conditions the fracture toughness of the matrix alloy is higher compared to that of the composite material [8, 9].

Thus it can be said that the target of the paper is twofold: The determination of the characteristics of the process zone and their dependence on the thickness of the specimen in case of MMCs and, on the other hand, the study of the mechanisms leading to failure, in an attempt to understand the deterioration of the mechanical characteristics of MMCs in the presence of macro-cracks.

2. Some theoretical considerations

It is accepted that in Linear Elastic Fracture Mechanics, a single parameter can characterize in a satisfactory manner the singular stress and strain fields around a crack tip. This parameter is usually described in terms of a balance of energy rates, which leads to the energy release rate concept, uniquely related to the stress intensity factor. Following a similar procedure for the case of nonlinear materials, the J-contour integral (or simply the J-integral) was introduced [10], which describes the flow of energy into the tip region. With respect to a point s on the crack front in a nonlinear elastic material, the J-integral is defined by the formula:

$$J(s) = \int_{\Gamma} \left(W\delta_{1j} - P_{ji}\frac{\partial u_i}{\partial X_1} \right) n_j d\Gamma - \int_{A_\Gamma} \frac{\partial}{\partial X_3} \left(P_{3i}\frac{\partial u_i}{\partial X_1} \right) dA. \tag{2.1}$$

In the above Eq. (2.1) Γ is an arbitrary curve enclosing the crack front at the position given by s, in the plane $X_3 = 0$, A_Γ is the surface area defined by Γ, W is the deformation work per unit volume, u is the displacement vector, P_{ij} denotes the Piola–Kirchhoff stress tensor, X_i is a component of the position

vector of a material point in the undeformed configuration and n_j is a component of a unit vector perpendicular to Γ.

For the Double Edge Notched Tensile (DENT) specimen, used for the determination of the J-integral in the experimental program of the present work, RICE [11] introduced the following simplified formula for J-integral:

$$J_R = \frac{K_I^2}{E} + \frac{1}{\ell_0 t_0}\left(2\int P du_P - P u_P\right). \tag{2.2}$$

Here K_I is the stress intensity factor, E the Young's modulus, P the applied load and u_p the plastic displacement. For this type of specimen the stress intensity factor, K_I, is given as [12]:

$$K_I = \frac{P}{t_0}\sqrt{\frac{\pi\lambda}{2w_0(1-\lambda)}}\left(1.122 - 0.561\lambda - 0.205\lambda^2 + 0.471\lambda^3 + 0.190\lambda^4\right). \tag{2.3}$$

In Eq. (2.3) w_0 is the half-width of the plate while $\lambda = a_0/w_0$, where a_0 is the initial crack length.

The validity of the J-integral approach was the subject of a long series of papers. The point most intensively criticized was related to the fact that it is strictly founded exclusively for nonlinear elastic materials, which are of reversible nature concerning the loading-unloading path. It appears thus that using the J-integral for elastic-plastic materials is illegitimate and the concept is applicable only until no unloading occurs in any part of the material, or in other words until crack propagation starts. Other points related to the difficulties encountered during the practical determination of the critical value of J-integral and the necessity to combine the experimental results with finite element analysis are of rather minor importance.

The consensus reached today is that the J-integral can be calculated at the tip of a crack even for an elastic-plastic solid until the crack starts propagating subject to the additional condition that the crack tip finite strain zone, in which damage occurs, is sufficiently confined. Indeed, the loss of constraint, appearing with large scale yielding, is directly related to the deviation of the relationship between the J-integral and the Crack Tip Opening Displacement (δ_t) from the one proposed by SHIH [13], even for a stationary crack:

$$J = \frac{\sigma_0 \delta_t}{d_n}. \tag{2.4}$$

The above Eq. (2.4) was obtained by Shih using the HRR solution for the stress and strain fields, which is valid within the framework of the deformation theory of plasticity, assuming that no unloading occurs. The flow behaviour of the material

is simulated by a power law, generalized as follows:

$$\varepsilon_{ij} = \frac{3}{2}\alpha \left(\frac{\sigma_e}{\sigma_0}\right)^{n-1} \frac{S_{ij}}{E}, \tag{2.5}$$

where ε_{ij} and S_{ij} are the components of the strain- and of the deviatoric stress-tensor, respectively, σ_e is the effective stress, defined as $\sigma_e = [3/2(S_{ij}S_{ij})]^{1/2}$, σ_0 is a reference value for the stress (usually defined as the 0.2% offset yield strength) and α, n are experimentally defined constants. Assuming then that the above restrictions are fulfilled, the stress field components, σ_{ij}, can be described according to Shih's approach by the following equation:

$$\sigma_{ij} = \sigma_0 \left(\frac{EJ}{\alpha\sigma_0^2 I_n r}\right)^{1/(n+1)} \tilde{\sigma}_{ij}(n, \theta), \tag{2.6}$$

where r is the radial distance from the crack tip, I_n is a dimensionless constant which depends on strain hardening and $\tilde{\sigma}_{ij}$ is, also, a dimensionless constant depending on strain hardening and angle θ from the crack plane. Concerning the function $d_n = d_n(n, \varepsilon_0)$ of Eq. (2.4), which was given by Shih as a nomogramme, OMIDVAR'S *et al.* [14] approximate solution was adopted in the present study, according to which it holds that:

$$d_n(n, \varepsilon_0) = \frac{\sigma_0}{E}^{1.05/(n-0.1)} \left(1 + \frac{3}{n}\right). \tag{2.7}$$

It is to be emphasized at this point that the previous analysis is valid as long as each material point experiences proportional loading. For cracked bodies this is not the case, since an intense strain region exists, within $\sim 2\delta_t$ of the tip, that experiences highly non-proportional loading. In such a case the analysis is only valid as far as the intense strain region is surrounded by a region in which the HRR model assumptions still prevail. This is true as long as δ_t is relatively small compared to both the crack size and the uncracked ligament length. Otherwise fracture toughness becomes strongly geometry-dependent [15]. The validity of the above assumption will be checked experimentally in the next paragraphs.

3. Experimental procedure

3.1. The material

The material used in the present study is the BP-2124 Al-Cu particulate MMC, produced by a powder metallurgy process. According to this process, aluminum alloys are reinforced with extremely fine silicon carbide (SiC) particles. The chemical composition of the matrix alloy is listed in Table 1. The respective

Table 1. The chemical composition of the BP-2124 Al-Cu alloy.

Element	Wt [%]
Copper	4.0–4.4
Magnesium	1.3–1.6
Manganese	0.4–0.7
Iron	0.3 max
Zinc	0.25
Silicon	0.2
Chromium	0.1
Titanium & Zirconium	0.2
Others (each)	0.05 max
Others (total)	0.2 max
Aluminum	Balance

composite is obtained by adding to the matrix alloy about 20% wt of SiC particles of average diameter 3 μm [16].

The BP-2124 Al-Cu particulate MMC has very good specific properties (specific stiffness and high specific strength). Its absolute mechanical properties are considerably improved in comparison to the matrix alloy. As it can be seen from Table 2, in which the values of the modulus of elasticity, tension strength, torsion strength and ductility are recorded, the improvement varies between 37% for the modulus of elasticity and 50% for the strength under torsion. Of course as it is expected, the ductility of the composite material is about 27% lower compared to that of the matrix alloy [17].

Table 2. The average mechanical properties of the BP-2124 Al-Cu MMC and of the respective matrix alloy (properties measured along the rolling direction).

	Elastic Modulus [GPa]	Tensile Strength [MPa]	Torsional Strength [MPa]	Ductility [%]
2124 Alloy	80.0	435	505	6.7
2124 MMC	109.9	622	760	4.9
Change [%]	(37)	(43)	(50)	(–27)

According to the manufacturing process, the raw materials, i.e. the atomized aluminum alloy powder and the silicon carbide micrograt, are bought-in to an internal specification covering chemistry and size. The powders are then processed and blended to a homogeneous mixture. The mixed powders are then canned, degassed and hot isostatically pressed to full density using conventional aluminum powder metallurgy practices. The hot pressed billets are decanned and converted to wrought product using standard metal working equipment.

The material was available in rolled plates of thickness equal to $t = 12$ mm and rolled sheets of thickness $t = 1.2$ mm. After the specimens were cut from the plate and machined in their standardized shape (by removing away material in the thickness direction), they were subjected to heat treatment as it was suggested by the manufacturer. The procedure included solution treatment for ninety minutes at 505°C and then immediately cold-water quench. No visible distortion or surface cracking of the specimens was observed due to the quenching. Finally, the specimens were carefully polished in order to eliminate any scratches and similar irregularities from their surface.

However, it should be mentioned at this point that the above heat treatment procedure might be the reason for the generation of residual stresses, which are suspected to be responsible for many mechanical changes including anisotropy, especially in case of particulate reinforced MMCs. Although the analysis of the residual stresses is beyond the scope of the present paper, it is mentioned here that extensive study of the BP-2124 Al-Cu MMC with the aid of SEM and TEM techniques verifies the above option: The rupture of it is generally initiated in the matrix alloy in the immediate vicinity of the SiC particles. The dislocation density is much higher in the grains in contact with the particles. The cracks are initiated in this region because there are high residual stresses due to the coefficient of thermal expansion mismatch and the heat treatment procedure adopted [18].

3.2. Specimens and testing procedure

Three different types of specimens were employed:

- The first one included miniature Single Edge Notched (SEN) used for the determination of the Crack Tip Opening Displacement (CTOD) with the aid of the Scanning Electron Microscopy (SEM) technique. They were cut out from the rolled sheet and plates along the rolling direction. After they were machined to the required thickness, which varied between 1.2 and 3.5 mm (by removing away material in the thickness direction very slowly by mechanical milling), they were formed to the familiar dog-bone – like standardized geometry. Edge cracks were machined on one side of the specimens by means of a rotating slow cutting diamond disc of thickness 100 μm. The specific cutting procedure was chosen

since it creates cracks with minimal mechanical damage at their root. The width of the specimens was $w = 6.5$ mm, their thickness varied between $t = 1.2$ mm and $t = 3.5$ mm, while their gauge length varied between 65 and 70 mm. The initial length of the cracks, a_0, varied between 1 mm and 3 mm, yielding f values (ratio of width of the specimen over the length of the crack) in the range from about 0.15 to 0.45. The cracks were cut either perpendicular to the rolling and loading direction ($\beta = 90°$) or inclined at 60° with respect to it ($\beta = 60°$).

These miniature specimens were subjected to in-situ, monotonically increasing tensile loading in the Scanning Electron Microscope (SEM), Cambridge S4-10 type, available at the Laboratory of Testing and Materials of the National Technical University of Athens. The level of the tensile loading is servo-controlled (patent of the Institute of Physics, London, UK). The maximum capacity of the loading device is 2.2 kN. Following the above procedure it becomes possible to measure *in situ*, with the maximum possible accuracy, the current CTOD. However, it is emphasized that if the exact shape of the crack tip were taken into account, the term describing better the quantity measured would be "Notch Root Opening Displacement" (NROD).

As far as it concerns the method for the measurement of CTOD, a procedure similar to the one described in ref. [8] was adopted, based on continuous monitoring and successive photograph of the specimen at various stages of the testing procedure. The measurements were carried out by means of a Gruman-type visioscopic fringe analyzer, equipped with a digital electronic micro-positioning system, of maximum error ± 0.5 μm.

- The second type included Double Edge Notched Tensile (DENT) specimens of length 150 mm and width 60 mm, the thickness of which varied again between 1.2 and 3.5 mm. They were cut from the rolled plates along the rolling direction and the load was induced along the same direction. The width of the ligament was kept constant equal to 20 mm since it was not among the purposes of the paper to study the influence of the length of the ligament on the process. The edge cracks of initial length $a_0 = 20$ mm were machined using the above described procedure for the same reasons. During the numerical analysis of the experimental results it was verified that path-independence at cracking initiation was secured and no case was detected for which the whole ligament length underwent finite strains.

The specimens were subjected to static tensile loading with the aid of a very stiff hydraulic frame. The crosshead speed did not exceed 0.02 mm/min. The load-displacement curve was recorded by means of very sensitive extensometers. The onset of fracture was detected by the appearance of thumbnails on the crack front at the center of the plates.

- The third type included prismatic specimens with orthogonal cross-section of constant width $w = 9$ mm and thickness varying from $t = 1.2$ mm to $t = 9$ mm,

for the determination of the dependence of fracture strength and ductility on the specimen thickness. They were cut either along the rolling direction or perpendicular to it or inclined 45° with respect to it, in order to study, also, the influence of the plastically induced anisotropy on the ductility and fracture stress. They were prepared very carefully to ensure parallel gauge length and faces that were orthogonal to the plane of the sheet.

A system of 8 strain gauges bonded in the mid-section of the specimens was used to measure in real time the transverse and the through-thickness strains as well as the longitudinal ones, which are necessary for the determination of the constitutive law. Gauges were bonded on all four sides of the specimens to monitor possible bending parasitic effects. A series of successive loading-unloading loops was executed in each experiment, in order to measure the pure elastic constants of the material as well as the plastic portion of strains. It is to be mentioned at this point that considerable difficulties were encountered during the measurement of strain in the case of very thin specimens, the maximum thickness of which did not exceed in any case 1.2 mm. Bonding gauges on such thin surfaces is not possible and uncertainties appear concerning the validity of the results. For these specimens the strains were measured using two alternative methods, one based on laser technology and a purely mechanical one based on conventional extensometers. The differences recorded between the two methods were insignificant.

4. Experimental results

4.1. SEN specimens and the critical COD

In Figures 1 (a, b) characteristic SEM photographs are displayed showing the unloaded tip of a crack (Fig. 1a) and the same tip immediately before final failure (Fig. 1b), for a crack oriented perpendicularly to the loading direction ($\beta = 90°$), with a crack length-to-width ratio $f = 0.3$. On the other hand, in Figs. 2 (a–c) characteristic SEM photographs are displayed showing the unloaded tip of a crack (Fig. 2a) and the same tip immediately before final failure (Fig. 2b), for a crack oriented at a direction $\beta = 60°$ with respect to the loading axis and $f = 0.3$ again. The photographs in Figs. 1 (a, b) and 2 (a, b) correspond to a magnification ratio equal to 500, while that in Fig. 2c corresponds to a magnification equal to 1000 giving a better view of the damaged zone around the tip.

From the series of SEM photographs taken during the loading process the CTOD was measured, adopting the procedure indicated in Figs. 3 (a, b), where 1 and 2 indicate characteristic material features on the specimens. Characteristic results are shown in Fig. 4, in which the CTOD is plotted versus the exter-

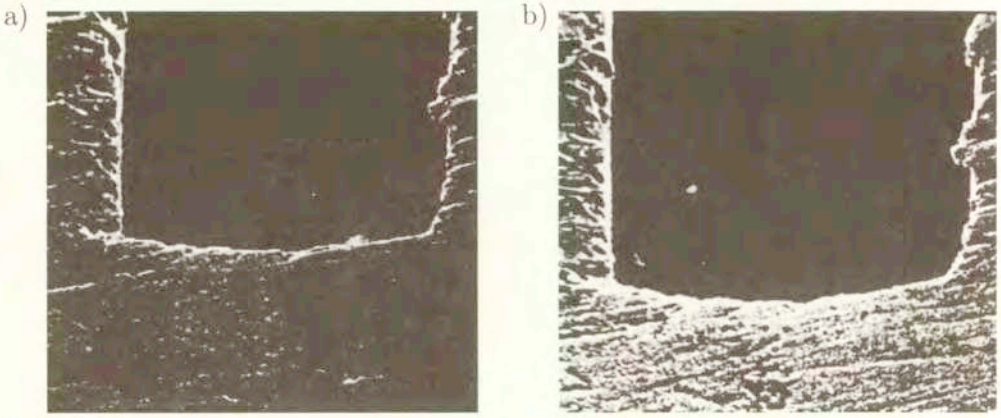

FIG. 1. SEM photographs of a crack with $\beta = 90^0$ (magnification 500×): a) Zero loading step. b) Final loading step.

nally applied net stress reduced over its corresponding maximum value, for the thinnest specimens, i.e. the ones with thickness $w = 1.2$ mm. In this figure filled symbols correspond to specimens with $\beta = 90°$ while empty symbols correspond to specimens with $b = 60°$. It is seen from this figure that the evolution of CTOD is almost negligible for load levels lower than half the final net fracture stress and then it increases in an exponential manner until the fracture stress is reached.

The above behaviour is qualitatively identical with the respective one described by KOURKOULIS in ref. [8] where a different technique for the measurement of COD was adopted, based on a modified δ_5 technique. In Fig. 5 results taken from [8] are shown concerning the COD values reduced over the initial width of the crack, for a crack with $\beta = 90°$, for both the composite material and the matrix alloy, for comparison reasons. Considering the initial width of the crack in [8] ($\delta_0 = 0.2$ mm), the absolute COD values reported there are of the order of 80 μm. Extrapolating these results at the tip of the crack the values of CTOD obtained vary in the range between 15 μm and 25 μm, in very good agreement with the results of the present study, for specimens of the same thickness.

As far as it concerns the dependence of the critical CTOD on the thickness of the specimen, it was concluded that an almost linear relationship exists, for the range of thickness studied in the present series of experiments. This linear relationship is clearly depicted in Fig. 6, in which the values of the critical CTOD are plotted versus the thickness of the specimen, for both the composite material and its respective alloy. As it can be seen from this figure, the critical CTOD increases linearly with increasing thickness from an initial value of 18 μm for

$t = 1.2$ mm to a final value of about 30 μm for $t = 3.5$ mm for the composite material. On the other hand, for the matrix alloy the respective values vary between 72 μm and 97 μm.

Finally, it was concluded that the average values of the critical CTOD appear to be independent of the value of f, for all specimen thicknesses, at least for the values of f used in the present study.

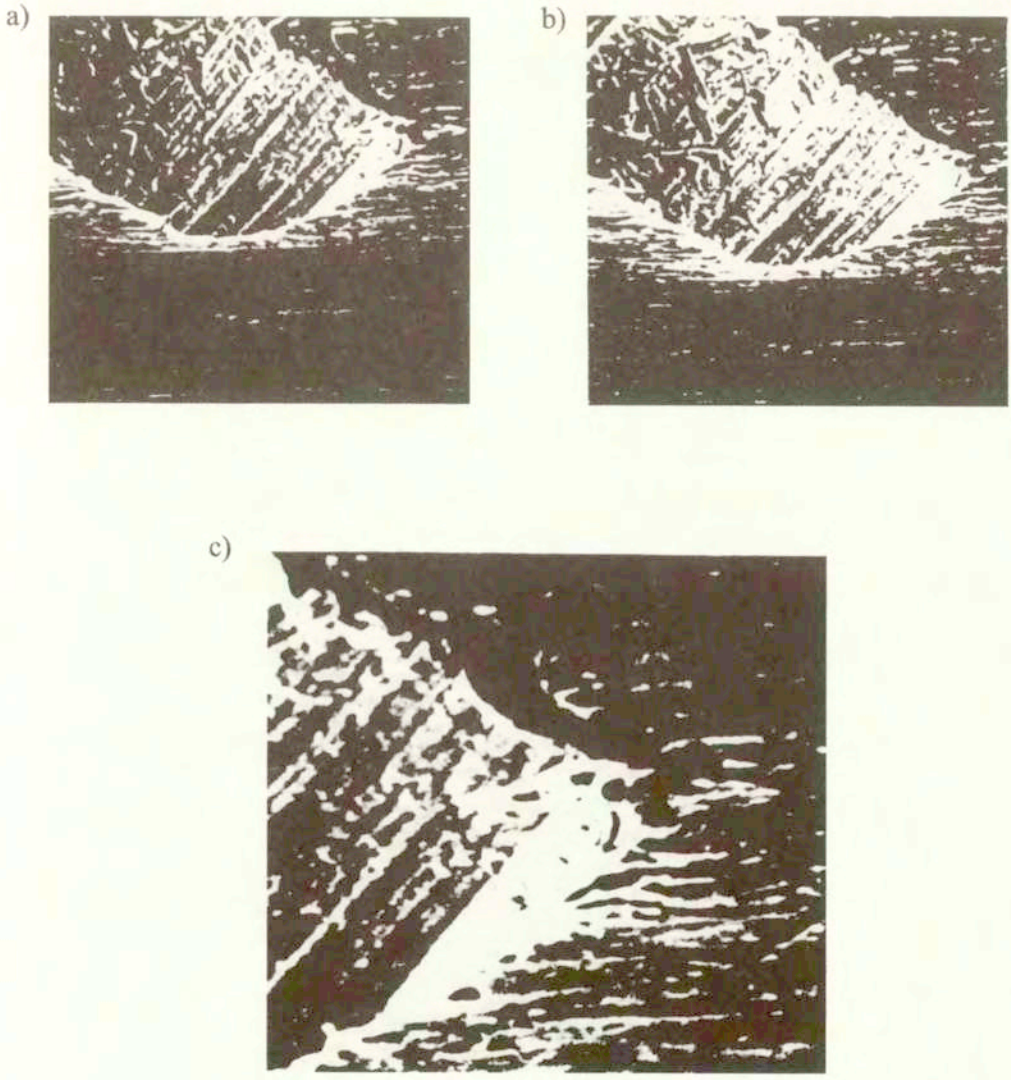

FIG. 2. SEM photographs of a crack with $\beta = 60°$: a) Zero loading step (magnification 500×). b) Final loading step (magnification 500×). c) Detailed view of the crack-tip area at the final loading step (magnification 1000×). Localized damage at the "corner" of the notch root is clearly visible.

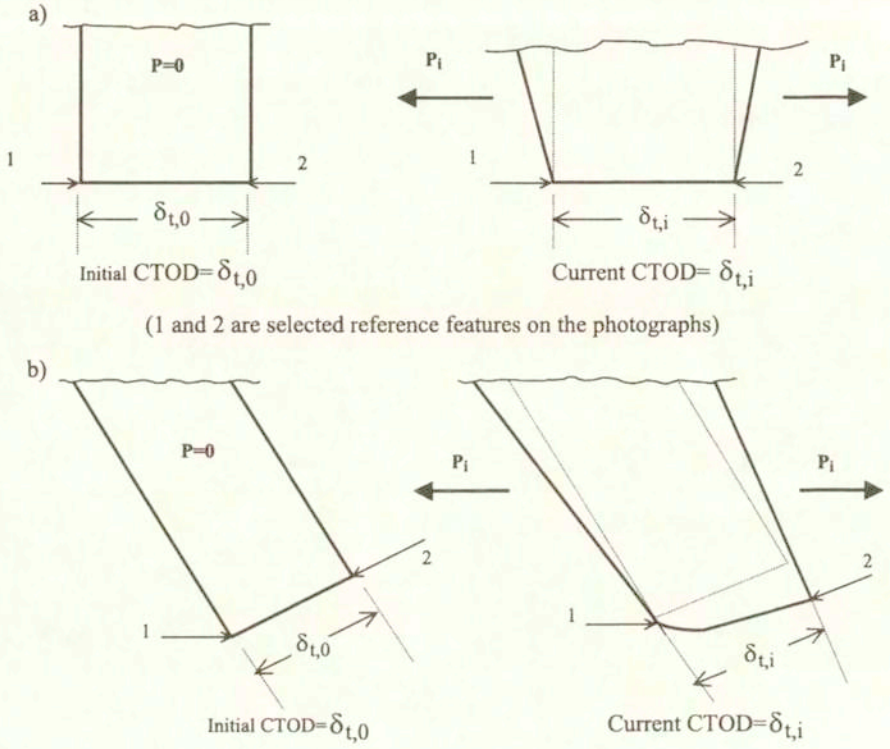

FIG. 3. The procedure followed for the measurement of the CTOD from the SEM photographs.

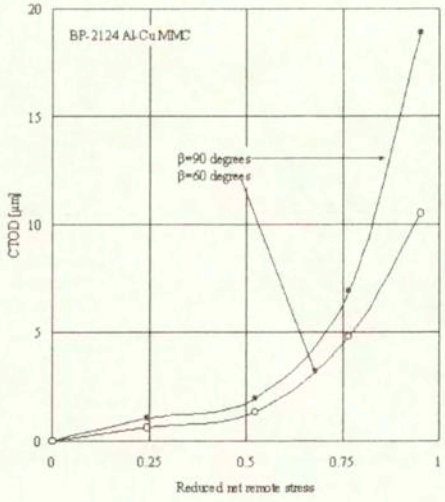

FIG. 4. CTOD versus the net remote stress for cracks with $\beta = 90°$ (filled symbols) and $\beta = 60°$ (empty symbols).

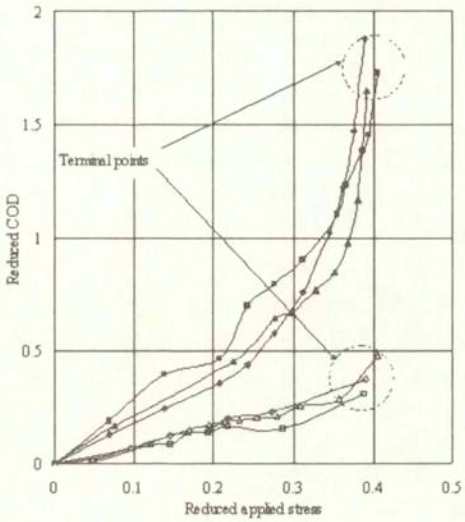

FIG. 5. COD vs. applied stress for $\beta = 90°$. Empty symbols represent the 2124 MMC and filled ones the respective alloy [8].

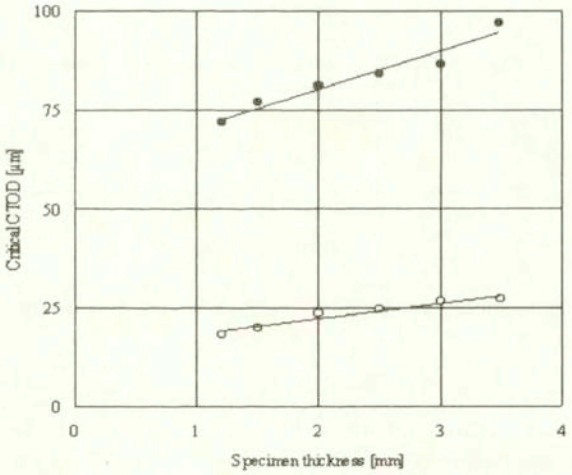

FIG. 6. The dependence of the critical Crack Tip Opening Displacement on the thickness of the specimens. Empty symbols correspond to the 2124 MMC and filled ones to the respective alloy.

4.2. DENT specimens and the critical J-integral

In order to determine the critical values of the J-integral, the DENT specimen configuration was used since the symmetry characterizing it renders numerical simulations easier. The numerical analysis employed is similar to the one followed

by PARDOEN *et al.* [6], based on the 3D domain integration technique introduced by SHIH *et al.* [19]. According to it $J(s)$ is computed from various contours in order to check the path-independence and a mean value is obtained by averaging the local values on the entire thickness. However, it is to be mentioned that the differences detected between these local values were relatively small for all specimens. As it was mentioned earlier, path-independence at the moment of crack propagation onset was observed for all geometries tested. Alternatively, the J-integral was determined using Eq. (2.2) together with the experimental results for the load – displacement curves. It is encouraging for the validity of the numerical analysis that the differences detected between the values obtained from the two alternative methods were very small and the maximum discrepancy did not exceed 4% in any case.

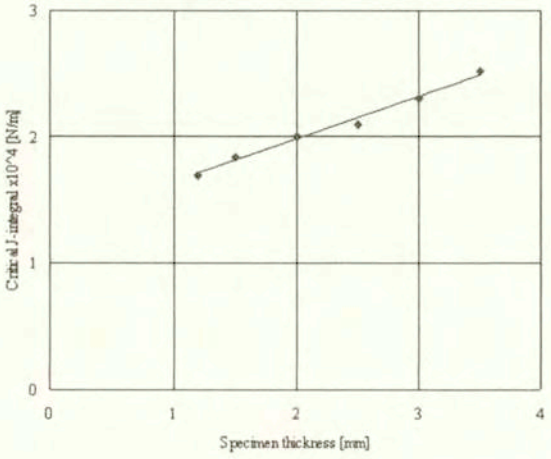

FIG. 7. Numerically calculated critical values of the J-integral versus the thickness of the specimen.

The results of the numerical analysis for the composite material are plotted in Fig. 7. As it can be seen from this figure, the critical values of J-integral increase linearly with increasing thickness, in a manner similar to Crack Tip Opening Displacement. However, it is to be mentioned that the line is of rather abrupt inclination although the material is rather brittle. Indeed the values vary from about 1.7×10^4 N/m for the specimens with $t = 1.2$ mm to about 2.5×10^4 N/m for the specimens with $t = 3.5$ mm. Such a behaviour is rather unexpected since the material studied here is less ductile compared to the one studied by PARDOEN *et al.* [6] for which the maximum value was reached for a thickness of about 5–6 mm. Such a trend is not detected for the material studied in the present work. However, it could be explained on the basis of the different

failure modes activated in case of pure metallic materials and composite ones, as it will be discussed in the next paragraph. In any case it is obvious that additional analysis is required (including also the tests with thicker specimens) in order to determine the exact form of the relation between J_C and specimen thickness.

The conclusions for the matrix alloy are of the same qualitative nature, however the slope of the $J_C = J_C(t)$ function is much higher.

4.3. Intact specimens

As a first experimental observation it should be mentioned that the axial strains measured in the rolling plane, $\varepsilon_{\text{axial},rp}$, diverge slightly, but systematically, from the axial strains measured in the thickness plane, $\varepsilon_{\text{axial},tp}$, for the same load level. The divergence becomes higher with increasing width-to-thickness ratio, as it can be seen from Fig. 8, in which the ratio $\varepsilon_{\text{axial},rp}/\varepsilon_{\text{axial},tp}$ has been plotted versus the axial stress, for a series of characteristic experiments with prismatic specimens cut and loaded along the rolling direction. Also, it is observed from the same figure that while $\varepsilon_{\text{axial},rp}$ exceeds $\varepsilon_{\text{axial},tp}$ during the initial loading steps, however, as the load increases, the phenomenon is inversed and tends to be eliminated as the load approaches the failure limit. The above observations indicate a non-uniformity of the deformation along the thickness of the plates, which becomes more pronounced as the thickness of the specimens increases. The conclusions for the other two types of prismatic specimens, namely the ones cut perpendicular to the rolling direction and diagonal to it, are of similar qualitative nature.

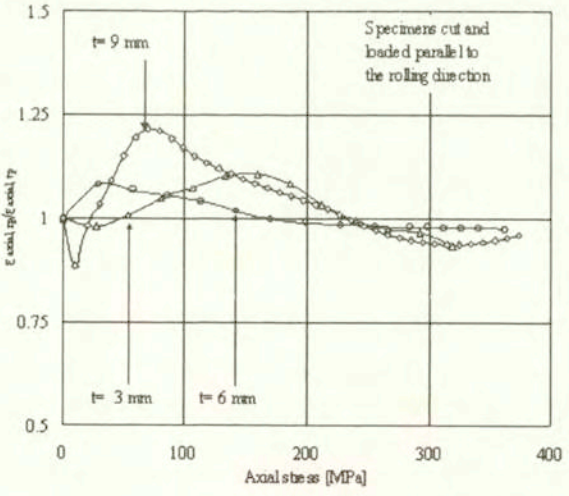

FIG. 8. The divergence between the axial strains measured in the rolling- and in the thickness-plane for specimens cut and loaded along the rolling direction.

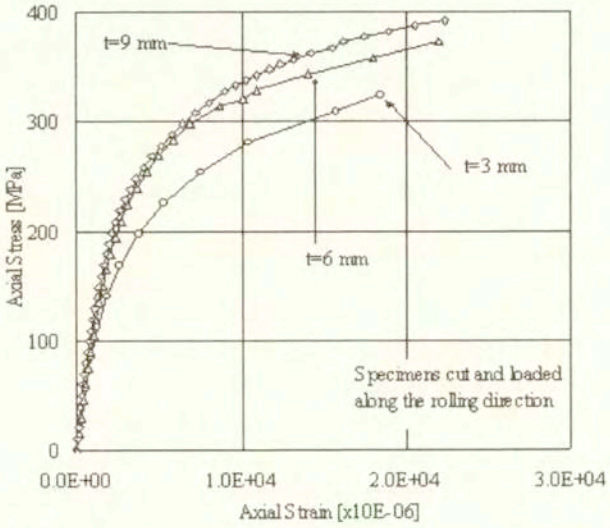

FIG. 9. The axial stress versus the axial strain measured in the rolling plane for prismatic specimens cut and loaded along the rolling direction.

As far as it concerns the variation of the fracture strength and ductility with specimen thickness it was concluded that both quantities increase with increasing thickness. In Fig. 9 characteristic axial stress – axial strain curves are plotted for the specimens cut and loaded parallel to the rolling direction. The axial strains were measured in the rolling plane. It can be seen from this figure that, contrary to the observations by ASSERIN–LEBERT *et al.* [20], the deviation between the graphs starts relatively early, namely almost immediately after surpassing the linearity limit. Such a behaviour seems to contradict common sense, however it can be explained if one takes into account that the material studied here is not a homogeneous continuum medium due to the presence of the reinforcing dispersed phase of the silicon carbide particles. The conclusions for the specimens cut and loaded perpendicular and inclined at 45° with respect to the rolling axis are almost identical. The respective results are summarized in next Figs. 10 and 11 for all types of specimens.

In Fig. 10 the fracture stress is plotted versus the specimen thickness for all three types of prismatic specimens. It is seen from this figure that the fracture stress–specimen thickness curve is almost linearly increasing with increasing thickness for thicknesses between $t = 1.2$ mm and $t = 5$ mm. From this point on the linearity is lost and the curve reaches its maximum value for specimens with thickness about 9 mm. The absolute differences between the fracture strength of the thinnest and thickest specimens was about 40% for all three types of specimens.

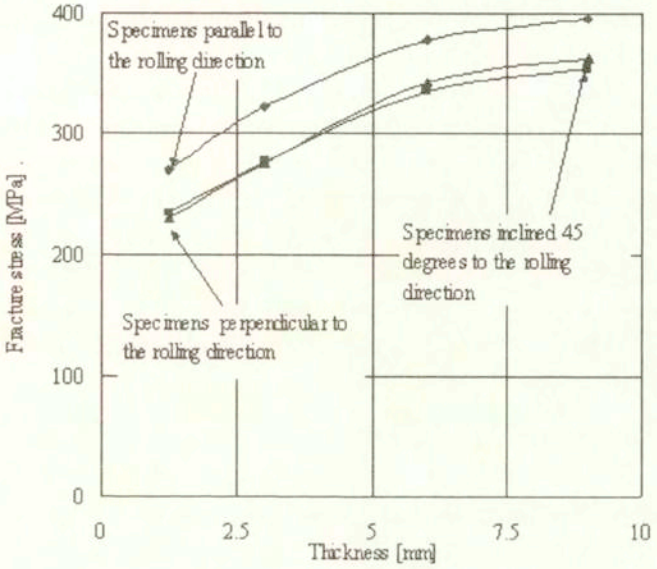

FIG. 10. The dependence of fracture stress on the specimen thickness.

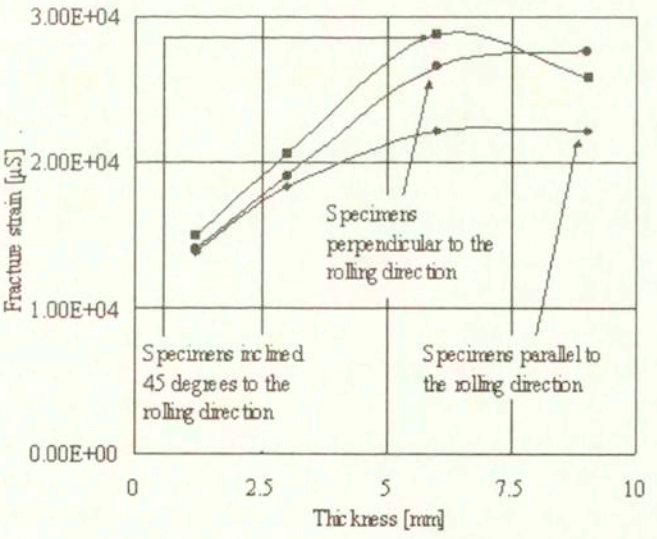

FIG. 11. The dependence of the ductility on the specimen thickness.

Concerning the influence of plastically induced anisotropy it is seen from Fig. 10 that the rolling direction is the strongest one while the differences between the other two directions are negligible no matter what the thickness of the specimen is.

In the next Fig. 11 the dependence of the fracture strain on the specimen thickness is plotted for all types of prismatic specimens. Although the qualitative behaviour of the graph is similar to that of the fracture stress, it is worth to be mentioned here that the specimens cut along the direction inclined 45° with respect to the rolling one appear to be the most ductile, especially for small thickness and they reach their respective maximum value of ductility already for a thickness equal to about 6 mm. Concerning the absolute differences they vary from about 80% for the specimens cut perpendicular to the rolling direction to about 50% for the ones cut parallel to it.

5. The fracture surfaces and the fracture mode

In Figs. 12 and 13 microfractographs are shown taken from two different locations of the fracture surface of a typical specimen with $\beta = 90°$ and $f = 0.3$. Indeed, in Fig. 14, in which the specific specimen is shown, the plane-stress "macromode" of fracture ahead of the crack tip (inclined plane of fracture) can be clearly detected. This failure mode is a combination of a shear component (distinguished by the shear lips) and a normal one (normal cone). The shear component prevails close to the surface layers whereas the normal one prevails at the mid-thickness layers of the specimen. The microfractograph of Fig. 12 corresponds to points of the shear failure area while the one of Fig. 13 to points of the normal failure one. From these figures it is safely concluded that the overall failure process is a ductile plane-stress one with an additional feature: The "dimple microfailure mode" is active. This is attributed to the microvoid coalescence mechanism, on which the ductile macrofracture of metals [21] is based.

Figures 12 b and 13 b were taken with the aid of the signal differentiation processing mode, by which contour enhancement or edge sharpening of the dimples is achieved. In this way one can better distinguish the differences in the morphology between the two areas of the failure surface (shear lips and normal cone). It can be observed from them that the shear prevailing area is characterized by an elongated dimple pattern, in contrast to the normal cone area which is characterized by a more or less "quasi-equiaxed" dimple pattern. Such a behaviour is attributed to the loss of severity of the triaxiality of the stress state near the surface layers of the material [22].

a)

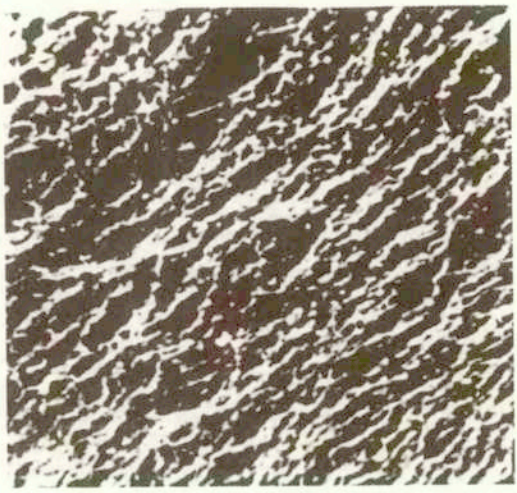

b)

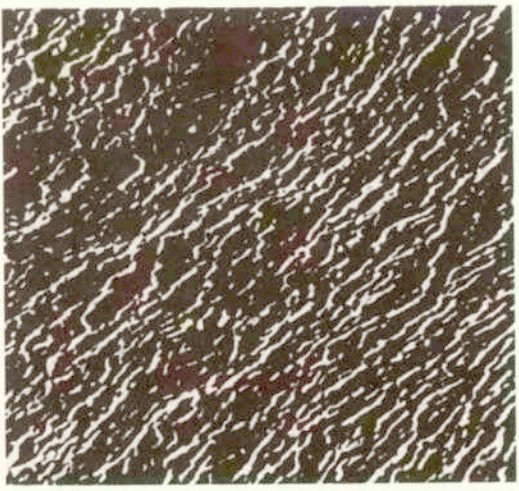

FIG. 12. SEM micro-fractographs (magnification 500×): a) Elongated shear dimpled surface. b) Signal processed image for the enhancement of elongated pattern.

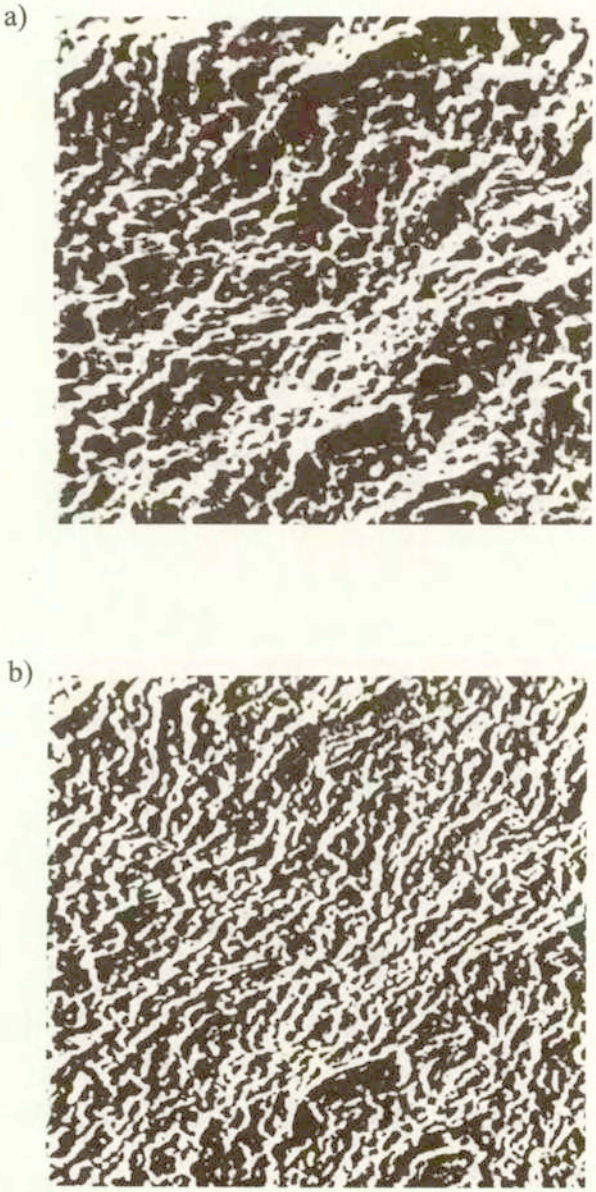

FIG. 13. SEM micro-fractographs magnification 500×): a) "Quasi-equiaxed" dimpled surface. b) Signal processed image for the enhancement of "quasi-equiaxed" pattern.

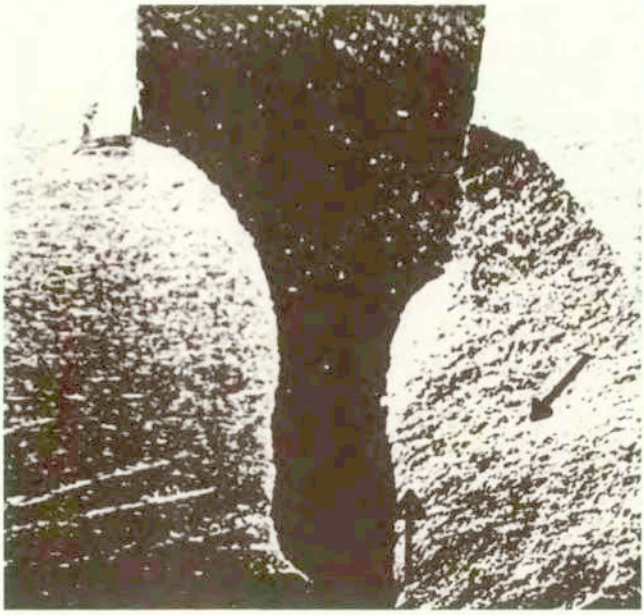

FIG. 14. SEM photograph of the fractured specimen. The arrows indicate the exact points at which the photographs of Fig. 12 (filled arrow) and Fig. 13 (empty arrow) were taken.

6. Conclusions

Some characteristics of the process zone developed around the tip of cracks as well as the fracture strength and ductility of the 2124 Al-Cu MMC were studied in the present work. The fractography of the fracture surfaces was used in order to determine the failure mechanisms activated.

The values of the critical CTOD recorded were less than 30 μm for the composite material and less than 100 μm for the matrix alloy. It is thus concluded that the intensively damaged zone surrounding the tip is restricted to less than about 2% of a_0 for the SEN specimens, for both the composite material and the respective alloy. Hence the HRR model appears to be valid, at least for the range of f values tested, although the failure mode detected is a ductile one. It means that Eqs. (2.6), (2.7) can be safely used for the description of the stress field for both materials.

It was also concluded that both the critical CTOD and the critical J-integral depend almost linearly on the thickness of the specimen. However, the experimental study did not employed specimens of increased thickness in order to determine the above quantities under plane strain conditions since it is not possible to apply the loads required to cause failure *in situ* on the Scanning Electron

Microscope. This was possible only for the fracture strength and ductility since the respective tests were executed using conventional hydraulic loading frames. For these quantities it was verified that after an initial linear portion of the respective graph, the increasing tendency was eliminated and a maximum value was reached for specimens with thickness about 9 mm for the fracture stress and of about 6 mm for the ductility. Additionally it is mentioned that the above quantities strongly depend on the orientation of the specimen with respect to the rolling direction, indicating the importance of the plastically induced anisotropy due to the manufacturing process adopted for the production of the composite material. The dependence for the matrix alloy is almost insignificant. This behaviour should be expected since in the case of the composite material, the plastically induced anisotropy is caused by the fact that the initially spherical reinforcing particles are transformed gradually into elliptic-paraboloidal ones [23]. Such a transformation does not take place in the matrix alloy and thus the plastically induced anisotropy is much weaker.

On the other hand, the analysis of the SEM images pointed out that the fracture process is still controlled by the void coalescence mechanism despite the presence of the reinforcing SiC particles. On the other hand, SEM analysis of the fracture surface of uncracked specimens indicated that the micro-cracks are initiated in the matrix rather than at the particle-matrix interface. This peculiar, at least for MMCs, phenomenon can be explained by the fineness of the reinforcement phase as well as by the process used for the production of the specific MMC (powder metallurgy) which is responsible for some porosity. Thus, in the case of uncracked specimens void nucleation than void coalescence is the critical step for failure. When the local plastic relaxation that relieves stress concentration becomes difficult, as in the case of pre-cracked specimens, where it is concentrated in the vicinity of the tip of the macroscopic crack, then the final failure occurs at rather low strains. It seems thus that the presence of macro-cracks changes the failure mechanism, explaining in this way the deterioration of the mechanical properties of cracked MMCs.

References

1. H. M. WESTERGAARD, *Bearing pressures and cracks*, Transactions of the ASME, **61**, A49–A53, 1939.

2. G. R. IRWIN, A*nalysis of stresses and strains near the end of a crack transversing a plate*, J. Appl. Mech., **24**, 361–364, 1957.

3. H. L. EWALDS, R. J. H. WANHILL, *Fracture mechanics*, Edward Arnold Publishers, London, 1985.

4. J. L. BLUHM, *A model for the effect of thickness on fracture toughness*, ASTM Proc., **61**, 1324–1331, 1961.

5. J. L. SWEDLOW, *The thickness effect and plastic flow in cracked plates. Aerospace Research Laboratories*, Office of Aerospace Research, U.S. Air Force, Wright-Patterson Air Force Base, OH, 1965.

6. T. PARDOEN, Y. MARCHALL, F. DELLANNAY, *Thickness dependence of cracking resistance in thin aluminium plates*, J. Mech. Phys. Solids, **47**, 2093–2123, 1999.

7. K. G. KREIDER, *Introduction to metal matrix composites*, [in:] Composite Materials, L. J. BROUTMAN and R. H. CROCK [Eds.], vol. **4**, chap. 1, Academic Press, New York, 1974.

8. S. K. KOURKOULIS, *The influence of cracks on the mechanical behaviour of particulate MMCs: an experimental study*, Arch. Mech., **53**, 439–456, 2001.

9. G. HENESS, L. GAN, Y. W. MAI, *Effect of particle morphology on matrix constraint in metal matrix composites*, 9th Int. Conf. of Fracture, Sydney, Australia, B. L. KARIHALOO [Ed.], Pergamon Press, **1**, 759–765, New York 1997.

10. J. R. RICE, *A path independent integral and approximate analysis of strain concentration by notches and cracks*, J. of Appl. Mech., **35**, 379–386, 1968.

11. J. R. RICE, *Elastic – plastic models for stable crack growth*, Proc. of the Conference on Mechanics and Mechanisms of Crack Growth, Churchill College, Cambridge, England, 14–39, 1973.

12. T. L ANDERSON, *Fracture mechanics – fundamentals and applications*, CRC Press, Boca Raton, 1995.

13. C. F. SHIH, *Relationships between the J-integral and the COD for stationary and extending cracks*, J. Mech. Phys. of Solids, **29**, 305–326, 1981.

14. B. OMIDVAR, M. P. WNUK, M. CHOROSZYNSKI, *Relationship between the CTOD and the J-integral for stationary and growing cracks*, Int. J. of Fracture, **87**, 331–343, 1997.

15. A. SCHAPERY, *Report MM5762-88-1*, Texas A&M University, College Station TX, 1988.

16. Particulate Metal Matrix Composite Processing Handbook, Issue 1, BP Metal Composites, Farnborough, England, 1991.

17. S. K. KOURKOULIS, N. P. ANDRIANOPOULOS, *Some Critical Aspects of the Mechanical Behaviour of Metal Matrix Composites*, Proc. 1st Nat. Conf. on Composite Materials and Structures, 57–71, S. A. PAIPETIS and E. E.GDOUTOS [Eds.], Kyriakidis Brothers S.A., Xanthi, Greece, 1997.

18. B. DODD, *Workability of metals and MMCs, in particular Al-Li alloys and Al-based composites*, Final technical Report of the EU project BREU-CT91-0398: BE4500-90, 50–51, 1994.

19. C. F. SHIH, B. MORAN, T. NAKAMURA, *Energy release rate along a three dimensional crack front in a thermally stressed body*, Int. J. Fract., **30**, 79–102, 1986.

20. A. ASSERIN-LEBERT, F. BRON, J. BESSON, A. F. GOURGUES, *Rupture of 6056 aluminum sheet materials: Effect of sheet thickness on strain localization and toughness*, Proc. ECF-14: Fracture Mechanics Beyond 2000, EMAS Publishing, Sheffield, England, **1**, 97–103, 2002.

21. Fractography and materials science, ASTM-STP 733, 1981.

22. S. K. KOURKOULIS, V. KYTOPOULOS, *Experimental quantification of crack tip parameters for particulate metal matrix composites*, Proc. of the 6th Congress of the Hellenic Association of Theoretical and Applied Mechanics, Thessaloniki, Hellas, **1**, 339–347, 2001.

23. S. K. KOURKOULIS, *Quantifying the plastic anisotropy for particulate Metal Matrix Composites*, Advanced Composites Letters, **11**, 153–163, 2002.

Received December 13, 2002.